Experimental Comparison of Control Strategies in a Single-Phase Grid-Feeding Converter for Microgrid Applications

Agustín Tobías, Víctor Cárdenas, Fernando Quiroz-Vázquez, Juan González-Rivera, Daniel Martínez-Padrón
Universidad Autónoma de San Luis Potosí, Engineering Department
Av. Dr. Manuel Nava 8, 78290, San Luis Potosí, México
Email: agustin.tobias@outlook.com, vcardena@uaslp.mx, fernando.iqv@gmail.com,
glzrivera04@gmail.com, daniel.stingmtz@gmail.com

***Abstract*—Nowadays, power electronics converters used in distributed generation have became a common tool to exploit the benefits of renewable energy sources, like solar energy via photovoltaic panels. The increase of using this kind of systems, working together in parallel operations as a microgrid (MG) in low voltage distribution networks, makes necessary accomplish certain control tasks in order to inject the available power to the grid, achieving a proper power sharing as long as maintaining the grid voltage and frequency among suitable levels for the whole operation system. The above mentioned is possible through the use of control strategies that allow the system obtain an adequate transient and steady state performance. This paper presents an experimental comparison between the performance of current decoupled control and passivity based control strategy, to inject active a reactive power using a power electronics converter working as a grid-feeding interconnected to the main grid focused to MG applications.**

***Index Terms*—Photovoltaic systems, power quality, grid-feeding, nonlinear control, passivity based control.**

I. Introduction

The increase of distributed generation with photovoltaic systems as a part of a microgrid, is facing some issues associated to high penetration levels in low voltage networks as voltage and frequency variations, proper power sharing problems and the capacity to operate in isolated or interconnected mode. These difficulties nowadays have been being solved through the modification of standards and local regulations to allow the users to get high quality of electric services.

The functions that the power electronics converters must fulfill to solve the presented problems, depend on their control objectives of each system in a MG: they can be working as grid-feeding, grid supporting and grid-forming converters [1]. The grid-feeding has an important role when is necessary to inject active and reactive power to the main grid.

One of the solutions for the aforementioned situations is implementing hierarchical control strategies, which gives to the system the necessary characteristics for accomplish each task, with a distributed generation system as a part of the main grid [2]. In these control structures, the local control of each converter has to be capable to receive the reference signals from the higher control level, and for this purpose, an appropriate local control strategy is needed in order to guarantee the system works as expected.

Different studies have reported linear and nonlinear control strategies applied to the local control level, where a typical linear control strategy is the current decoupled control with cascade PI control loops [3], [5], since it is possible to operate in closed-loop to achieve a desired performance [4], whereas a common limitation comes from a limited performance when the system operates outside the linear region, as well as disturbances sensitivity and parameter dependency. These type of limitations can be improved using non linear control strategies as passivity based [6] and sliding modes controllers [7].

This paper selects a current decoupled control strategy (CDC) and a passivity based control strategy (PBC), in order to compare the advantages and disadvantages faced when both have to accomplish the injection of active and reactive power to the grid as long as the power electronics converter is grid synchronized being capable to operate as a grid-feeding converter. The results achieved were obtained as follows: Section II contains the mathematical system model developed in a synchronous reference frame; Section III presents the control laws applied to the system; Section IV contains the simulation of the control strategies to check their functions are fulfilled; Section V transient and steady state experimental results are obtained to conclude the advantages or disadvantages of the system working in the conditions imposed.

II. Modeling of the System

Fig. 1 shows a full-bridge single-phase grid tied converter. The system considers an output L-C-L filter to provide higher harmonic attenuation than a common L filter. Also, it takes advantage of its characteristics as the size, cost and weight reduced [8]. $R_{1,2}$ are the parasitic resistance of the inductors (Ω), $L_{1,2}$ are the inductance (H), R_f is the parasitic resistance of the capacitor and C_f is the capacitance (F) of the output filter. C_{dc} is the capacitance of the DC voltage source (F), i_{PV} is the current of the photovoltaic array (A), i_{dc} is the DC

978-1-7281-8987-1/20/$31.00

current injected to the grid-feeding converter (A), V_{dc} is the DC voltage source (V) , and v_g is the AC voltage (V) of the main grid. It is important to mention that v_{dc} is regulated by a DC-DC converter which is capable of obtain the MPP of a photovoltaic array. This work considers the DC-AC converter receives a regulated voltage from a DC source with finite output impedance.

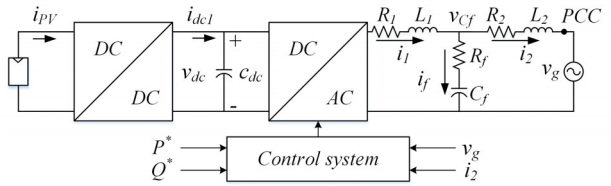

Fig. 1. Single-phase grid-feeding converter.

The average mathematical model obtained in a synchronous reference frame of the system in Fig. 1, takes into account the parasitic resistance in the passive elements of the LCL filter. The losses of the power electronics devices are neglected [9] and the model is given by:

$$L_1\frac{di_1^d}{dt} = -\left(R_1+R_f\right)i_1^d + R_f i_2^d - v_{C_f}^d + u^d v_{CD} + \omega L_1 i_1^q, \tag{1}$$

$$L_1\frac{di_1^q}{dt} = -\left(R_1+R_f\right)i_1^q + R_f i_2^q - v_{C_f}^q + u^q v_{CD} - \omega L_1 i_1^d, \tag{2}$$

$$L_2\frac{di_2^d}{dt} = R_f i_1^d - \left(R_2+R_f\right)i_2^d + v_{C_f}^d - v_g^d + \omega L_2 i_2^q, \tag{3}$$

$$L_2\frac{di_2^q}{dt} = R_f i_1^q - \left(R_2+R_f\right)i_2^q + v_{C_f}^q - v_g^q - \omega L_2 i_2^d, \tag{4}$$

$$C_f\frac{dv_{C_f}^d}{dt} = i_1^d - i_2^d + \omega C_f v_{C_f}^q, \tag{5}$$

$$C_f\frac{dv_{C_f}^q}{dt} = i_1^q - i_2^q - \omega C_f v_{C_f}^d, \tag{6}$$

$$C_{cd}\frac{dv_{cd}}{dt} = i_{dc1} - \frac{1}{2}\left(u^d i_1^d + u^q i_1^q\right), \tag{7}$$

where ω is the angular frequency of the main grid (rad/s), v_{Cf} is the capacitor voltage, u^d and u^q are the modulation index of the PWM technique.

III. Control Strategies for the Full-Bridge Single-Phase Grid-Feeding Converter

The control strategies considered in the local level of a hierarchical control scheme of the grid-feeding converter, are developed in order to achieve an adequate performance when each converter supplies active and reactive power at the PCC. This control level makes possible to inject the available power according to the system conditions.

A. Current decoupled control strategy in a synchronous reference frame

The Current Decoupled Control strategy (CDC) developed in a synchronous reference frame, is one of the most common linear control schemes used to control power electronics converters, due to the suitable performance in the tracking and regulation of DC signals [3]. It is developed from the mathematical model of the converter in (1)-(7) and it is composed of PI controllers in a cascade loops array as shown in Fig. 2, where P is the active power (W), Q the reactive power (VAr), θ_g is the phase angle of the main grid and the superscript * stands for the reference values.

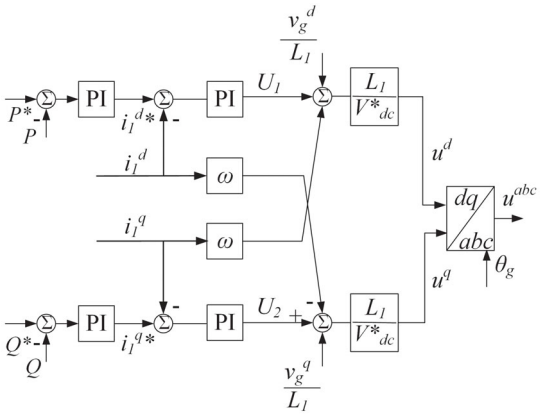

Fig. 2. Control block diagram of the current decoupled control strategy .

The control strategy according to Fig. 2 contains the non-linear terms that linearizes the system model [5], as long as considers i_1 as the output of the system to use only one current sensor for implementation purpose, improving the system reliability, and is represented as

$$u^d = \frac{L_1}{V_{dc}^*}\left[\omega i_1^q + \frac{v_g^d}{L_1} + U_1\right], \tag{8}$$

$$u^q = \frac{L_1}{V_{dc}^*}\left[-\omega i_1^d + \frac{v_g^q}{L_1} + U_2\right], \tag{9}$$

where $u^{d,q}$ are the control signals used in the modulation scheme, $v_g^{d,q}$ are the grid voltages in the synchronous reference frame, and $U_{1,2}$ represents the output of the proportional integral (PI) controllers in the inner current loops of the cascade control structure and they are

$$U_1 = k_{p1}(i^{d*} - i^d) + \frac{k_{i1}}{s}(i^{d*} - i^d), \tag{10}$$

$$U_2 = k_{p1}(i^{q*} - i^q) + \frac{k_{i1}}{s}(i^{q*} - i^q), \tag{11}$$

where k_{p1} and k_{i1} are the proportional and integral gains of the PI controllers respectively, i^{d*} and i^{q*} are the reference currents.

The closed loop transfer function of the current loops is

$$G_1(s) = \frac{i^d(s)}{i^{d*}(s)} = \frac{(k_{p1}s + k_{i1})}{s^2 + k_{p1}s + k_{i1}}, \tag{12}$$

and the transfer functions of the active and reactive power loops [10] are

$$\frac{P}{P^*} = \frac{k_{pp}v_g^d s + k_{ip}v_g^d}{\left(k_{pp}v_g^d + 2\right)s + k_{ip}v_g^d}, \tag{13}$$

$$\frac{Q}{Q^*} = \frac{k_{pq}v_g^d s + k_{iq}v_g^d}{\left(-k_{pq}v_g^d + 2\right)s - k_{iq}v_g^d}, \tag{14}$$

where k_{pp}, k_{ip} are the gains of the active power loop PI controller and k_{pq}, k_{iq} the gains of the reactive power loop PI controller.

B. Passivity Based Controller

Passivity based controller (PBC) strategy has been implemented in power electronics converters due to advantages over other control strategies, since it is possible to use energy information of physical systems and it is relatively easy to implement. The main control objective is to achieve *stabilization by passivation* using a storage function [11]. The design procedure of the PBC considers the model given by (1)-(7) in the following form:

$$\mathbf{M}\dot{x} + \mathbf{R}x + \mathbf{J}x = \varepsilon, \tag{15}$$

where the matrix $\mathbf{M}$ contains the storage energy elements with the restriction $\mathbf{M} > 0$, $\mathbf{R}$ is the damping matrix, and in this case, contains the parasitic resistances with $\mathbf{R} = \mathbf{R}^T \geqslant 0$; $\mathbf{J}$ results in an skew-symmetric matrix with the interconnection structure with $\mathbf{J} = -\mathbf{J}^T$, and ε is the non controlled inputs vector [11]. These matrices are given by

$$\mathbf{M} = \begin{bmatrix} L_1 & 0 & 0 & 0 & 0 & 0 & 0 \\ 0 & L_1 & 0 & 0 & 0 & 0 & 0 \\ 0 & 0 & L_2 & 0 & 0 & 0 & 0 \\ 0 & 0 & 0 & L_2 & 0 & 0 & 0 \\ 0 & 0 & 0 & 0 & C_f & 0 & 0 \\ 0 & 0 & 0 & 0 & 0 & C_f & 0 \\ 0 & 0 & 0 & 0 & 0 & 0 & C_{CD} \end{bmatrix}, \tag{16}$$

$$\mathbf{R} = \begin{bmatrix} R_1 & 0 & 0 & 0 & 0 & 0 & 0 \\ 0 & R_1 & 0 & 0 & 0 & 0 & 0 \\ 0 & 0 & R_2 & 0 & 0 & 0 & 0 \\ 0 & 0 & 0 & R_2 & 0 & 0 & 0 \\ 0 & 0 & 0 & 0 & 0 & 0 & 0 \\ 0 & 0 & 0 & 0 & 0 & 0 & 0 \\ 0 & 0 & 0 & 0 & 0 & 0 & 0 \end{bmatrix}, \tag{17}$$

$$\mathbf{J} = \begin{bmatrix} 0 & -\omega L_1 & 0 & 0 & 1 & 0 & -u^d \\ \omega L_1 & 0 & 0 & 0 & 0 & 1 & -u^q \\ 0 & 0 & 0 & -\omega L_2 & -1 & 0 & 0 \\ 0 & 0 & \omega L_2 & 0 & 0 & -1 & 0 \\ -1 & 0 & 1 & 0 & 0 & -\omega C_f & 0 \\ 0 & -1 & 0 & 1 & \omega C_f & 0 & 0 \\ u^d & u^q & 0 & 0 & 0 & 0 & 0 \end{bmatrix}, \tag{18}$$

$$\varepsilon = \begin{bmatrix} 0 & 0 & V_{red} & V_{red} & 0 & 0 & i_B \end{bmatrix}^T, \tag{19}$$

$$x = \begin{bmatrix} i_1^d & i_1^q & i_2^d & i_2^q & v_{Cf}^d & v_{Cf}^q & V_{dc} \end{bmatrix}^T. \tag{20}$$

The control strategy is derived from the following expression

$$\mathbf{M}\dot{X^*} + \mathbf{R}X^* + \mathbf{J}X^* + \mathbf{R_a}\mathbf{e} = \varepsilon, \tag{21}$$

where $\mathbf{X}^*$ is the desired variables vector, $\mathbf{R_a}$ is the desired damping, $\mathbf{e} = (x^* - x)$ is the error vector [8]. This control strategy is given by

$$u^d = \frac{1}{V_{dc}^*}\left[L_1\dot{i}_1^{d*} + R_1 i_1^{d*} - \omega L_1 i_1^{q*} + v_{C_f}^{d*} + k_1\left(i_2^{d*} - i_2^d\right)\right], \tag{22}$$

$$u^q = \frac{1}{V_{dc}^*}\left[L_1\dot{i}_1^{q*} + R_1 i_1^{q*} + \omega L_1 i_1^{d*} + v_{C_f}^{q*} + k_2\left(i_2^{q*} - i_2^q\right)\right], \tag{23}$$

where k_1 y k_2 are the selected values of the desired matrix damping [6], [9].

IV. Simulation Results

The performance of the control laws developed is demonstrated via simulation results to verify that both control strategies are capable to achieve the steady state conditions. The full system is integrated of the inverter and its controllers, and is implemented in PSIM software.

To guarantee the cascade loops array operation, the constant gains of the PI controllers in CDC strategy are selected to achieve a proper decoupling, where the inner loop must to operate with a one decade bandwidth lower than the switching frequency of the PWM strategy, and the outer loop must to operate with a one decade bandwidth lower than the bandwidth of the inner loops [6], as it is shown the Bode diagram in Fig. 3.

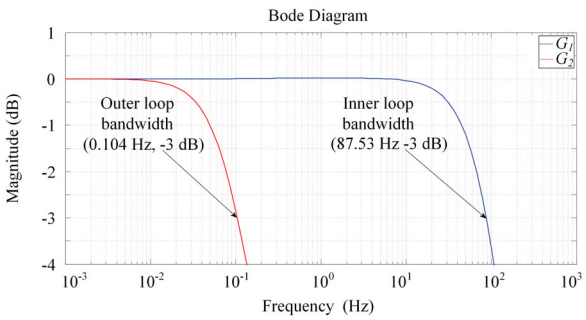

Fig. 3. Bode diagram of the closed loop transfer functions.

Table I contains the nominal parameters of the simulation and experimental system, where R_g and L_g are the impedance parameters considered for the grid.

A. Grid-Feeding Converter Injecting Active Power

This case considers the grid-feeding converter is injecting active power to the grid, and the transient response of each control strategy is measured when the power reference changes from 0 to 700 W at time $t = 0.05$ s. The signals taken in the simulation case are the output current i_2, the current signals in the synchronous reference frame $i_2^{d,q}$ and the active

TABLE I
SYSTEM AND CONTROL PARAMETERS

Parameter	Value	Parameter	Value
V_{DC}	250 V	f	60 Hz
V_{AC}	127 V_{rms}	f_{sw}	12500 Hz
P	700 W	R_1	142 mΩ
Q	$\pm$700 VAr	R_2	1.11 $m\Omega$
C_f	6.88 μF	L_1	3.03 mH
R_f	0.2 Ω	L_2	1.11 mH
R_g	77 $m\Omega$	L_g	612 μH
Simulation		**Experimental**	
CDC			
k_{p1}	440	k_{p1}	550
k_{i1}	40	k_{i1}	280
k_{pp},k_{pq}	0.0055	k_{pp},k_{pq}	0.0065
k_{ip},k_{iq}	0.055	k_{ip},k_{iq}	0.2800
PBC			
K_1	3	K_1	6
K_2	1.5	K_2	3

and reactive power error signals err_P and err_Q. The output impedance considered of the DC source is 2 Ω and allows verifying the performance of each control strategy when the DC bus is not well regulated. Figs. 4(a) and 4(b) show the transient response of the signals measured, where it is possible to observe that the CDC strategy achieves the steady state with a settling time $t_{ss} = 330$ ms, and the PBC has a settling time $t_{ss} = 22$ ms, which is faster than CDC strategy. Although both control strategies compute v_{dc} at its reference value, the PBC strategy has a steady state error due to the control law is not capable to achieve the power references when DC bus voltage decreases in opposite with the CDC which take advantage of the integral action of PI controllers.

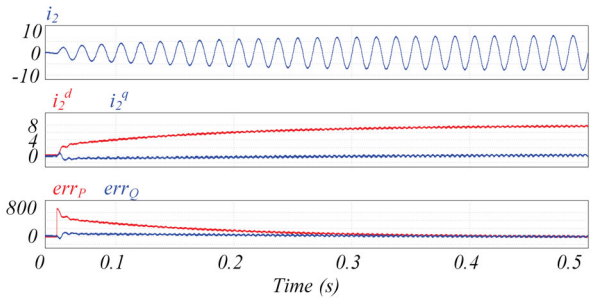

(a) CDC.

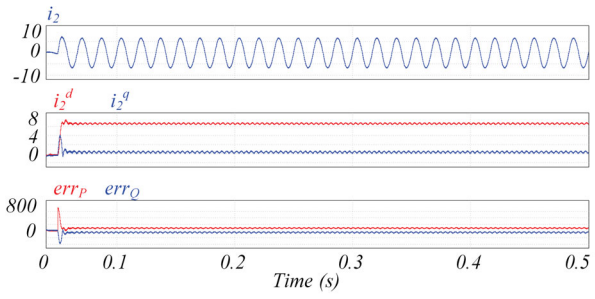

(b) PBC.

Fig. 4. Transient response of the grid-feeding injecting 700 W to the grid.

B. Power Quality Performance

The total harmonic distortion (THD) of the output current is obtained to evaluate the power quality performance in steady-state conditions. Table II contains the THD for different active and reactive power reference values. It can be observed that the PBC strategy achieves a better performance with THD values in the output current i_2 less than 4%.

TABLE II
STEADY-STATE SIMULATION VALUES.

P (W)	Q (VAr)	I_{rms} (A)	THD (%) CDC	THD (%) PBC
700	0	5.38	4.26	2.44
700	700	7.61	4.95	2.76
700	-700	7.61	5.58	2.86
300	300	3.26	5.41	3.32
300	-300	3.26	5.03	2.59
200	200	2.16	5.76	3.74
200	-200	2.16	4.85	2.49

V. EXPERIMENTAL RESULTS

The experimental results were obtained in different scenarios, carrying out transient performance tests and measuring harmonic components of the output current to calculate the THD values of each case. The experimental prototype is shown in Fig. 5, it is composed by a single-phase full-bridge converter connected through a LCL filter to the main grid, and the control strategies were implemented in a TMS320F28379D DSP. To verify the control strategies proposed above, the

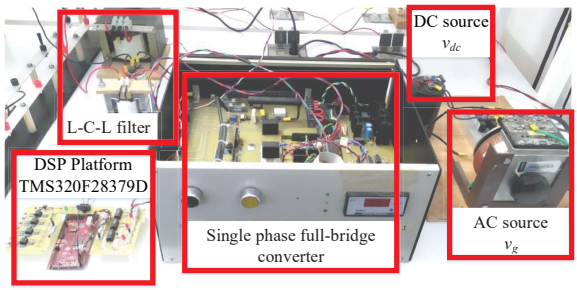

Fig. 5. Single-phase grid-feeding converter experimental prototype.

following experimental tests were carried out making an evaluation between the controllers performance during the transient response when the power reference change, and the THD of the current in steady-state, facing different active and reactive power scenarios. The signals measured in the experimental prototype are: Ch1 is the AC grid voltage v_g, Ch2 is the output current i_2, Ch3 is the DC bus voltage and Math. is the instantaneous active power given by Ch1 and Ch2.

A. Grid-Feeding Converter Injecting Active Power

This case illustrates the transient response of the grid-feeding converter for each control strategy. First, the system is synchronized and interconnected to the main grid and active and reactive power are not injected, with $P^* = 0$ W $Q^* = 0$ VAr in steady state conditions; after that the power reference

is changed to $P^* = 700$ W. Fig. 6(a) and Fig. 6(b) show the transient responses where the settling time is measured from the instant when the power reference is changed up to the instant when the injected power achieves the reference value. It can be seen that both control strategies have an adequate performance in both cases, with a settling time smaller than 3 cycles of the grid voltage; PBC has a faster response than the CDC.

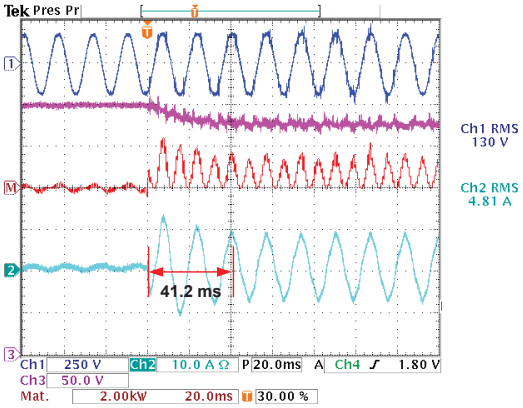

(a) CDC.

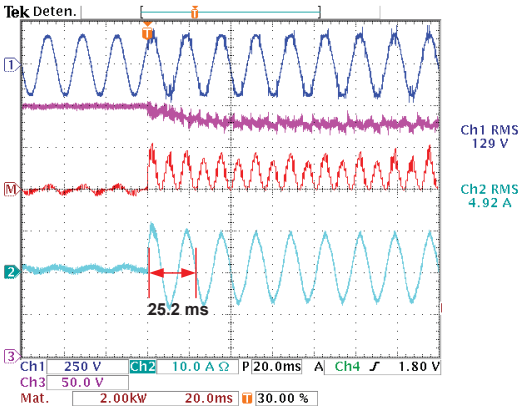

(b) PBC.

Fig. 6. Grid-feeding converter injecting active power.

B. Grid-Feeding Converter Injecting Active and Reactive Power

This case shows the system operation when the active and reactive power are changed from 0 up to the nominal values $P = 700$ W and $Q = 700$ VAr. Similar to the previous case, the system starts its operation without injecting power at steady state condition, but in this case, active and reactive power references change at the same time to obtain the transient response. The positive reactive power reference makes the grid-feeding converter have capacitive behavior also injecting active power. Fig. 7(a) and Fig. 7(b) show that both control strategies have a suitable performance, similar to the aforementioned case, but the responses in these cases are slower due to the higher level power reference demanded.

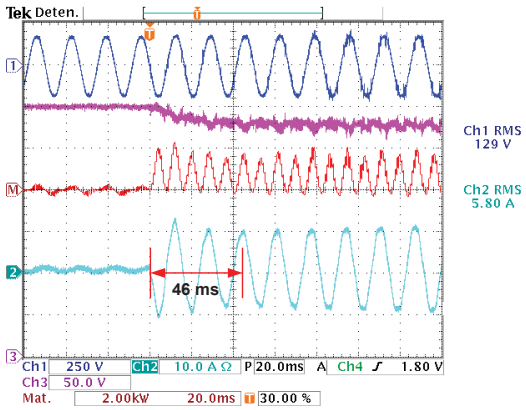

(a) CDC.

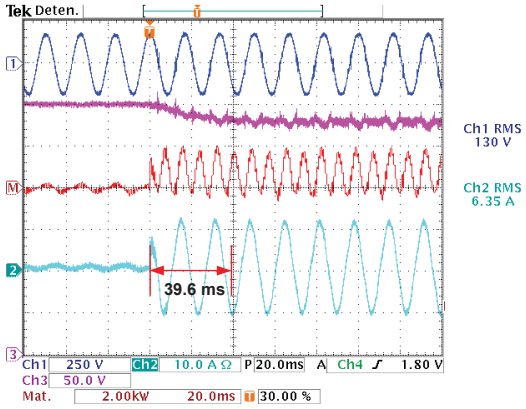

(b) PBC.

Fig. 7. Grid-feeding converter injecting active and capacitive reactive power.

C. Grid-Feeding Converter Injecting Active Power and Consuming Reactive Power

The transient response obtained in this case is produced when the active and reactive power references are changed from 0 to the nominal values, but at this time the reactive power reference has a negative value to give inductive behavior to the converter. Fig. 8(a) and Fig. 8(b) also show a suitable transient performance, and in this case, t_{ss} is 6.4 ms faster compared to the previous case because of an amount of the total reactive power is actually consumed by the filter's inductors. Table III contains the settling time t_{ss} obtained for each experimental case. It can be observed that the PBC achieve the steady state with a settling time in about on cycle less than CDC tests.

D. Power Quality Performance

The THD values of the current i_2 are calculated from the harmonic components measured for each case of power reference according to the Table IV. It can be observed that THD does not have a great difference between the control strategies, but their performance decrease with a lower power reference due to the radiated noise levels affect the sensor performance.

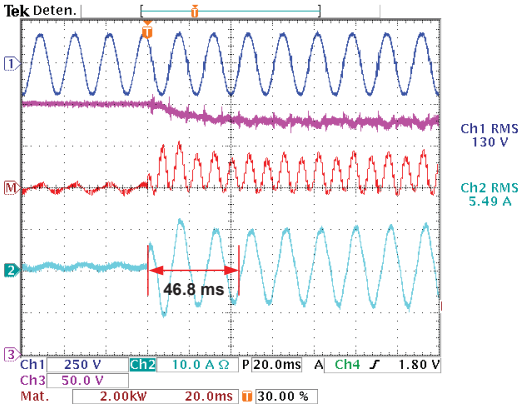

(a) CDC.

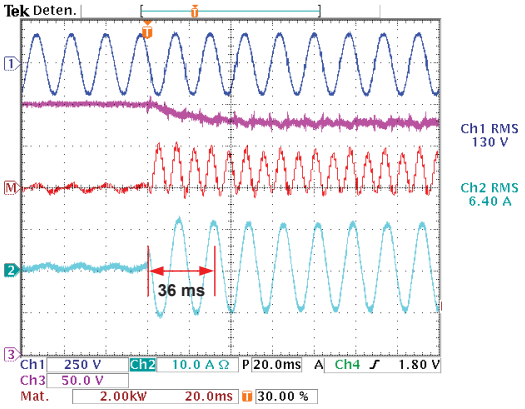

(b) PBC.

Fig. 8. Grid-feeding converter injecting active and inductive reactive power.

TABLE III
SETTLING TIME DURING PROPOSED TRANSIENT RESPONSES

CDC		PBC	
P =700 W Q =0 VAr			
t_{ss}	41.2 ms	t_{ss}	25.2 ms
P =700 W Q =700 VAr			
t_{ss}	46.8 ms	t_{ss}	39.6 ms
P =700 W Q =-700 VAr[a]			
t_{ss}	46 ms	t_{ss}	36 ms

[a]Minus symbol (-) denotes inductive reactive power

VI. CONCLUSIONS

The transient response during proposed power changes shows that PBC achieves a better performance with a smaller settling time compared with the CDC strategy transient response. However, in experimental cases the settling time obtained is not considerable bigger than three full cycles of the grid voltage. Furthermore, one of the drawback observed in the PBC, in simulation and experimental results, is that this control law is directly affected by the voltage changes due to the lack of a regulated DC bus. In this sense it is hard to achieve a well performed regulation task, in opposite with the current decoupled control strategy, which is able to achieve the power reference value settled, although the DC bus is not regulated at nominal value. The THD values do not have a significant difference between control strategies in each case of the experimental tests, but it increases due to the current sensor decrease its performance with lower current levels, which can be solved considering a better performed current sensor.

TABLE IV
STEADY-STATE EXPERIMENTAL VALUES.

P (W)	Q (VAr)	I_{rms} (A)	THD (%) CDC	THD (%) PBC
700	0	5.38	6.8	7.39
700	700	7.61	5.11	6.23
700	-700	7.61	6.43	5.59
300	300	3.26	11.77	14.56
300	-300	3.26	13.31	13.03
200	200	2.16	16.72	21.13
200	-200	2.16	19.28	17.88

REFERENCES

[1] J. Rocabert, A. Luna, F. Blaabjerg and P. Rodrguez, "Control of power converters in AC microgrids," in IEEE Transactions on Power Electronics, vol. 27, no. 11, pp. 4734-4749, Nov. 2012.

[2] A. Bidram and A. Davoudi, "Hierarchical structure of microgrids control system," in IEEE Transactions on Smart Grid, vol. 3, no. 4, pp. 1963-1976, Dec. 2012.

[3] M. Zarif, M. Monfared, "Step-by-step design and tuning of VOC control loops for grid connected rectifiers", International Journal of Electrical Power & Energy Systems, vol. 64, pp. 708-713, 2015.

[4] J. Alcalá, V. Cárdenas, A. Aganza, J. Gudiño-Lau, and S. Charre, "The performance of the BTB-VSC for active power balancing, reactive power compensation and current harmonic filtering in the interconnected systems". Energies 2020, vol. 13, 831, 2020.

[5] E. Rosas, V. Cárdenas, J. Alcalá and C. Núñez, "Active and reactive current decoupled control strategy applied to a single-phase BTB converter," 2009 6th International Conference on Electrical Engineering, Computing Science and Automatic Control (CCE), Toluca, 2009, pp. 1-6.

[6] Saumitra Barman, Soumya Samanta, Jyoti Prakash Mishra, Prasanta Roy, Binoy Krishna Roy, "Design and implementation of an IDA-PBC for a grid connected inverter used in a photovoltaic system," IFAC-PapersOnLine, vol. 51, no. 1, 2018, pp. 680-685.

[7] J. Hu, L. Shang, Y. He and Z. Q. Zhu, "Direct active and reactive power regulation of grid-connected DC/AC converters using sliding mode control approach," in IEEE Transactions on Power Electronics, vol. 26, no. 1, pp. 210-222, Jan. 2011.

[8] R. N. Beres, X. Wang, M. Liserre, F. Blaabjerg and C. L. Bak, "A review of passive power filters for three-phase grid-connected voltage-source converters," in IEEE Journal of Emerging and Selected Topics in Power Electronics, vol. 4, no. 1, pp. 54-69, March 2016.

[9] Fernando I. Quiroz-Vázquez, V. Cárdenas, J. González-Rivera, Mario González-García, Alejandro Aganza-Torres and Fortino Mendoza-Mondragón, "Inversor fotovoltaico monofásico interconectado a la red con soporte de potencia reactiva," Congreso Nacional de Control Automtico 2019, Puebla, México , pp. 55-60, Oct. 2019.

[10] R. Sierra, V. Crdenas, J. Alcal and N. Visairo, "Single-phase analysis of BTB converter under unbalanced voltage conditions," 2011 8th International Conference on Electrical Engineering, Computing Science and Automatic Control, Merida City, 2011, pp. 1-6.

[11] Romeo Ortega, Arjan van der Schaft, Bernhard Maschke, Gerardo Escobar, "Interconnection and damping assignment passivity-based control of port-controlled Hamiltonian systems," Automatica, Volume 38, Issue 4, 2002, pp. 585-596.